ERA, 31(4): 2337–2357.
DOI: 10.3934/era.2023119
Received: 29 November 2022
Revised: 16 February 2023
Accepted: 23 February 2023
Published: 27 February 2023

Electronic Research Archive

http://www.aimspress.com/journal/ERA

Research article

Investigation on the fractal characteristic of asphalt pavement texture roughness incorporating 3D reconstruction technology

Han-Cheng Dan[1,2], Yongcheng Long[1], Hui Yao[3,*], Songlin Li[1], Yanhao Liu[3] and Quanfeng Zhou[4]

[1] School of Civil Engineering, Central South University, Changsha, Hunan 410075, China
[2] Rail Data Research and Application Key Laboratory of Hunan Province, Central South University, Changsha, Hunan 410075, China
[3] Beijing Key Laboratory of Traffic Engineering, Faculty of Architecture, Civil and Transportation Engineering, Beijing University of Technology, Beijing 100124, China
[4] Zhonghai Construction Co., Ltd, Shenzhen, Guangdong 518057, China

* **Correspondence:** Email: huiyao@mtu.edu.

Abstract: The textural roughness of asphalt pavement surface is an important indicator to characterize pavement skid resistance. In this paper, multi-visual technology was applied to capture the surface image of asphalt pavement which was transformed into a visualized 3D point cloud model. Then, based on the principle of the digital elevation model (DEM), the disordered 3D point cloud is rasterized and projected into a 2D matrix which contains generalized point cloud elevation information. Meanwhile, the 2D matrix is transformed into grayscale to build the equivalent grayscale image. Furthermore, the fractal dimensions were calculated in terms of one-dimensional pavement section profile, two-dimensional grayscale, and equivalent grayscale to characterize the pavement roughness. The results showed that the fractal dimensions are positively correlated with the mean texture depth (MTD), and the fractal dimension of equivalent grayscale has the best correlation with MTD. It should be highlighted that the equivalent grayscale image is directly transformed by the reconstruction of the three-dimensional point cloud, and the grayscale value of each point can represent the elevation of different pavement surfaces. Therefore, the equivalent grayscale image can better reflect the real roughness of the pavement surface. Meanwhile, the proposed method in this paper can effectively reduce the influence of some factors (e.g., light and color, etc..) on the texture detection of the pavement surface.

Keywords: texture roughness; 3D reconstruction technology; fractal dimension; pavement texture;

equivalent grayscale; mean texture depth

1. Introduction

The surface texture and friction coefficient of asphalt pavements do not only affect driving comfort but also play an important role in traffic safety during vehicle acceleration and deceleration [1–3]. The texture characteristics of the surface are a crucial factor to ensure high anti-skid performance of asphalt pavement, however, the texture roughness of asphalt pavement contains significant randomness and complexity. In order to classify the texture characteristics of asphalt pavement with different aggregate gradations, the Permanent International Association of Road Congresses (PIARC) [4] defined pavement texture into four types according to the wavelength (wl) and amplitude (A) of the deviations, including micro-texture (0 mm< wl < 0.5 mm; 0.001 mm < A < 0.5 mm), macro-texture (0.5 mm < wl < 50 mm; 0. 1 mm < A < 20 mm), mega-texture (50 mm < wl < 500 mm; 1 mm < A < 50 mm), and roughness or unevenness (wl > 500 mm; 1 mm < A < 200 mm). In general, the micro-texture is affected by the surface properties of aggregates (e.g., mineral properties) and bituminous materials. Similarly, macro-texture is influenced by the mix properties of asphalt mixture, including the shape, size, and gradation of the aggregates [5,6]. In general, the mean texture depth (MTD) and mean profile depth (MPD) are usually used to evaluate the macro-texture [7]. The MPD is obtained by the laser in a two-dimensional scenario, while MTD is tested in three-dimensional by the sand patch method which can reflect more complex pavement surface in detail [8]. In other words, the MPD always reflects a two-dimensional profile of pavement surface, which cannot fully describe the three-dimensional characteristics of pavement texture. For instance, the MTD value is 0.6231 mm and MPD value is 1.7472 mm, which indicates the difference in the magnitude (Figure 1).

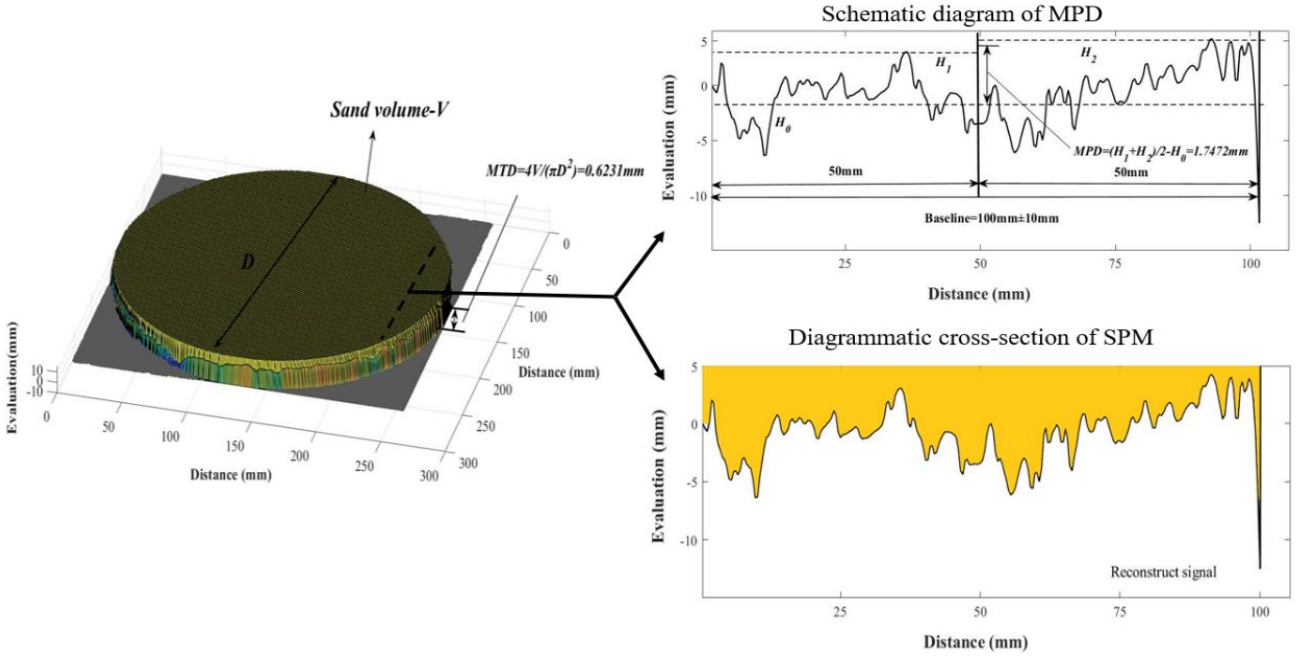

Figure 1. Schematic diagram for the difference between MPD and MTD.

Currently, the means for detecting pavement texture information are roughly divided into two categories, namely, direct and indirect measurement technologies, which can directly obtain the two-dimensional or three-dimensional morphology of the pavement surface. The direct measurement technologies (e.g., CT scanning, laser scanning, mechanical stylus and image processing) are intuitive and graphic which can be directly used for evaluating the texture characteristics of pavement surface [9–11]. The indirect measurement technology is to measure other indicators related to the pavement texture characteristics by simpler means (e.g., sand patch method, British pendulum tester and razor blade method) [11]. It should be pointed out that both of the direct and indirect measurement technologies have advantages and disadvantages [12]. For instance, most of the direct measurement technologies have the disadvantages of high cost (e.g., CT scanning and laser scanning measurement), but the measurement results tend to be more accurate and can better reflect the texture characteristics of pavement (e.g., CT scanning, Laser scanning and mechanical stylus) [13]. As for indirect measurement methods, the sand patch method is punctual, the lane must be closed, and not for a network level, etc.. Although the British Pendulum Tester is low cost and easy to operate, its measurement results tend to be influenced by the environment and are relatively less accurate [14]. Likewise, razor blade method is of high precision, but it has high requirements for optical environments, so it is not suitable for the field test [15].

The computer vision-based texture detection method is on the rise, including image processing technology and binocular stereo vision [16,17]. These technologies provided a new direction for pavement texture detection and the essence of which is the use of image processing techniques to extract useful information in the photograph. It has the advantages of simple equipment, low cost, easy operation, and labour-saving to non-destructively detect pavement texture on a large scale [18,19]. Zhang et al. [20] improved the threshold segmentation method to achieve effective segmentation of pavement texture images. An aggregate distribution uniformity index was proposed based on the number and location of texture, which can be used to comprehensively evaluate the aggregate distribution uniformity of asphalt pavement. Ghaderi and Abedini [21] analyzed two-dimensional digital images of airport asphalt pavement through three mainstream digital image processing methods, among which the calculation results obtained by the edge pixel number regression model and fuzzy logic edge detection method have a good correlation with MTD. Nevertheless, the existing image processing was based on a binary image or grayscale image. Since the color image information was underutilized to reduce the data loss in the process of image transformation, it thus leaded to insufficient accuracy of subsequent parameter calculation or model reconstruction. Therefore, the processing technology based on pavement surface images and the investigation on pavement texture characteristics needs to be further promoted and improved.

The primary objective of this paper is to present a new method to characterize the asphalt pavement surface texture. The method combines image processing techniques, 3D reconstruction techniques, and fractal theory. At first, the pavement surface will be reconstructed, and then the equivalent pixel matrix of grayscale is obtained to make a digitized pavement image which contains pavement texture information. Further, the texture distribution of asphalt pavement is then quantified after combined with fractal theory. Finally, the asphalt pavement texture is captured by the field test to demonstrate feasibility of the proposed method. Compared with traditional methods, the method in this paper is less costly and more efficient. The 3D reconstruction technology based on image processing can overcome the problem of insufficient accuracy in extracting pavement texture information from 2D digital images. Moreover, the 3D point cloud of pavement is rasterized and

grayed out, which can solve the problem of redundant and difficult to calculate 3D point cloud data. The proposed method is expected to provide a potential reference for quantifying asphalt pavement texture. The flow chart of this research is shown in the Figure 2.

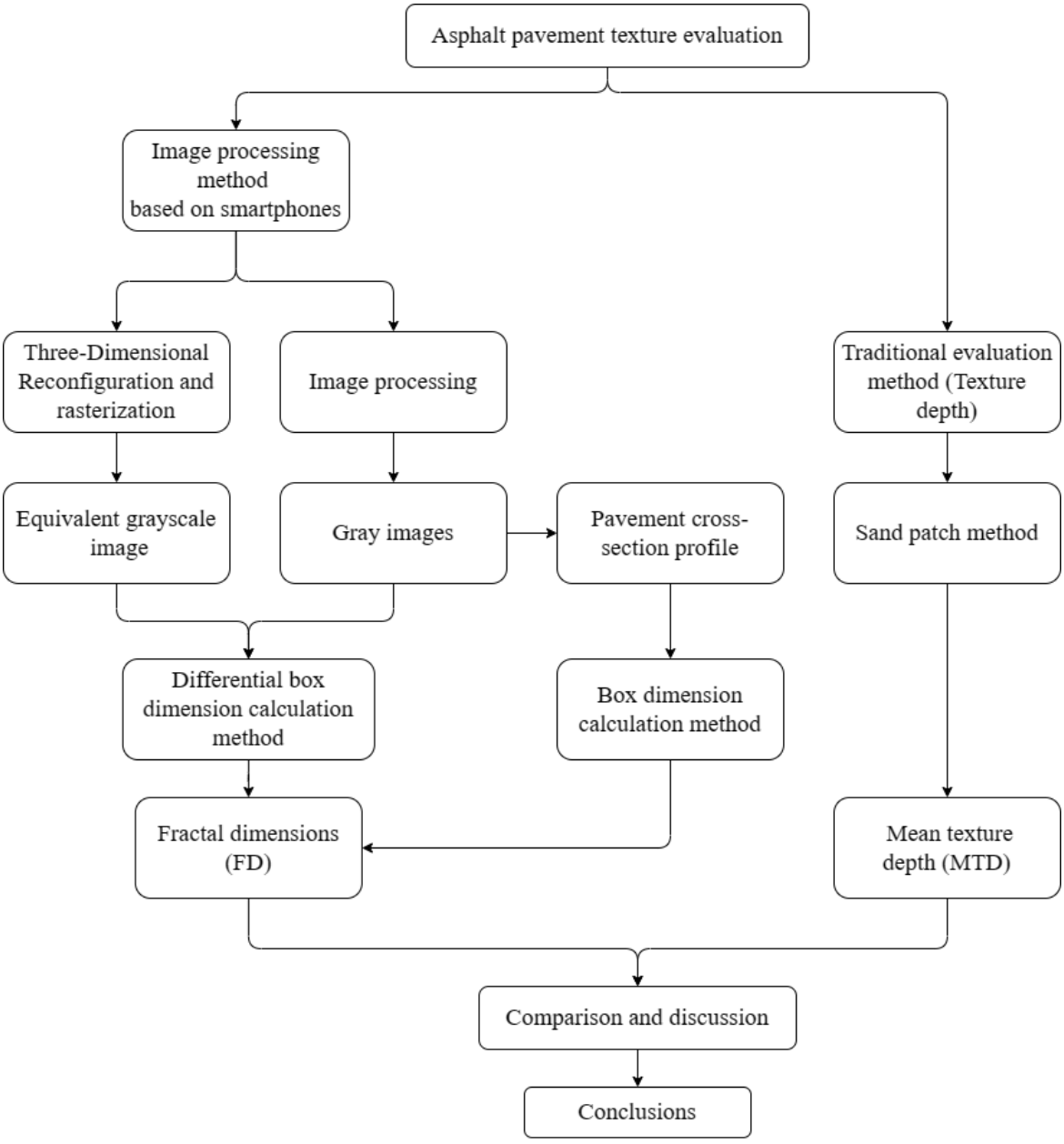

Figure 2. The flow chart of research.

2. Image acquisition and 3D reconstruction of pavement surface

2.1. Image acquisition

The first step is to acquire the image of asphalt pavement surface containing information such as geometrical morphology and spatial location of the measured objects. A mobile phone with a 12-

megapixel rear CMOS camera was used to capture pavement surface images. A pavement with open space, uniform lighting, and a flat surface was selected for shooting. It is better to keep the subject and background as separate as possible and minimize the influence of light and shadow on the inherent color. In addition, in order to characterize the realistic size, calibration points need to be placed in advance. Dan et al. [22] provided different styles of calibration points, consisting of a central point and two circles. Based on this principle, a square calibration plate of size 300 mm × 300 mm was designed and marked with calibration points on its four corners, the square calibration plate and the shooting methods is shown in Figure 3. To follow the principle of full coverage and high overlap, the camera height of photographing plane was 600 mm above the calibration plate and a total of 20–30 photographs were taken with a rotation angle of 45° (Figure 4). It should be pointed out that the number and angle of photos taken directly affect the accuracy of 3D reconstruction. Secondly, the camera baseline used for photography should not be too large, and the photographs taken should reflect the texture characteristics of the pavement as much as possible.

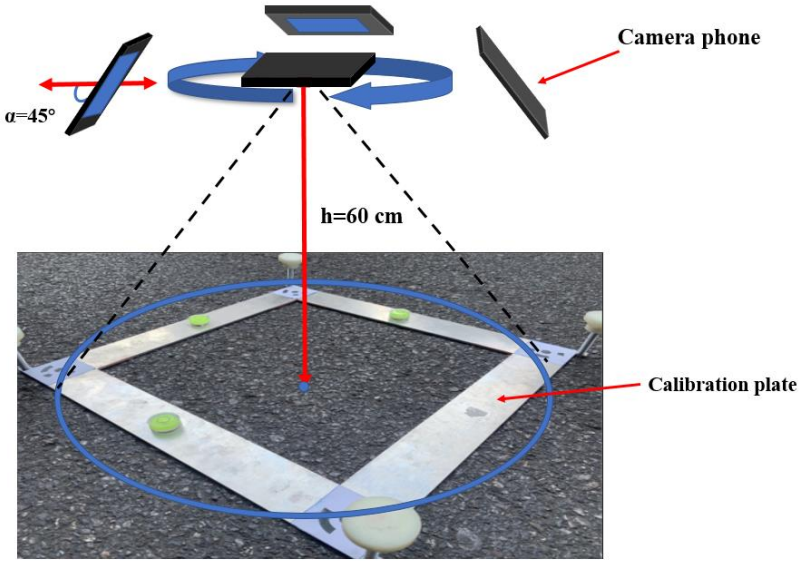

Figure 3. Schematic diagram of the square calibration plate.

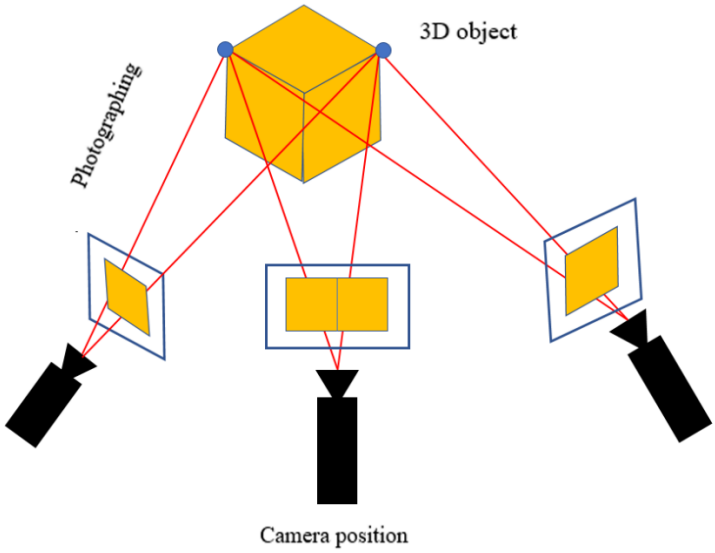

Figure 4. The diagram of the shooting position.

2.2. 3D morphology reconstruction of asphalt pavement surface

The determinants of whether the reconstruction model can be used to obtain the pavement texture depth are the accuracy of photograph matching and the accuracy of object characteristics. The structure-from-motion method (SFM) is suitable for photograph sets captured from multiple viewpoints, and the corresponding relationship of the same pixel points in the photographs can be obtained through the characteristic matching algorithm, and the three-dimensional coordinate information of spatial points can be obtained by using matching constraint relationship in combination with the principle of triangulation [22–24]. The 3D reconstruction technology based on multiocular vision and SFM can improve the accuracy and speed of identification of the characteristics of represented objects, allowing spatial information about the objects to be presented more accurately. Therefore, this technology is used in the three-dimensional reconstruction of the pavement structure herein.

Firstly, the captured image was adjusted to remove blurred or severely distorted images caused by misfocusing. In the second step, the connection points were matched between the key points and the captured photos to build a sparse point cloud and the camera positions were marked. In the third step, the coordinates of the calibration points were imported in the four corners of the calibration plate to scale the model to the real size. In the fourth step, the dense point cloud was generated. Three-dimensional point cloud reconstruction is shown in Figure 5. It is necessary to be pointed out that the detected mark position and real coordinates will have pixel-level errors, which are generated during photography and alignment. The photos with errors exceeding five pixels are eliminated, from which the overall non-linear optimization of the initial sparse point cloud results was then conducted to improve the accuracy of the established dense point cloud.

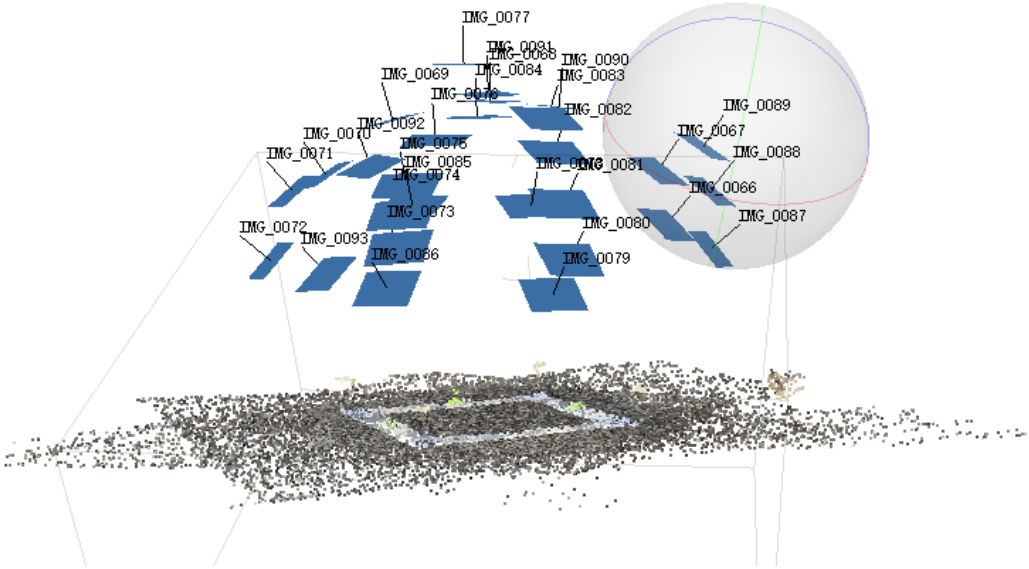

Figure 5. Three-dimensional point cloud reconstruction.

Moreover, the experimental results showed that the intensity of illumination and the photographic angle affect the accuracy and success rate of the reconstruction model. Therefore, in full light, a small aperture can be used to help eliminate false focus and photographic blur, a low ISO can be set to reduce noise, and a short exposure time can be used to prevent blur caused by jitter [25–27]. In this study, oblique photography was adopted and the external light source is natural light. On the one hand, for the possible front-light side and backlight side (shadow), the shadow will not change. On the other hand, since the photographing time of each photo was less than 1 second and less than 10 seconds were taken for each detection point, it can be considered that the light source position and lighting condition has no obvious change during the period of the photographic process [22]. Therefore, the modelling accuracy will not be affected accordingly. As a matter of fact, the reflection type of light on asphalt pavement is diffuse reflection. Regardless of whether the light source is oblique or not, there is no obvious shadow on the pavement surface except for the possibility of relatively dim light. However, blurry or distorted photographs may be rejected in the alignment stage (i.e., reconstruction may also fail if there are few valid photographs or a lack of different angles used).

2.3. Point cloud rasterization and pixel matrix output

The reconstructed 3D point cloud contains millions of $[x, y, z]$ disordered coordinate points, which needs to be converted into an easy-to-study pixel matrix output. In this paper, the point cloud was rasterized by combining the principle of the digital elevation model (DEM); Digital elevation model is a digital simulation (i.e., digital representation of terrain surface form) of ground terrain by finite terrain elevation data [28,29]. The rasterization process was dividing the point cloud data into several grid cells of equal size, and certain attribute values, such as elevation values, intensity values, etc., were put into the grid cells to form an image with a coordinate system. The basic method of dividing the grid is as follows:

$$\text{Cols} = \text{int}\left(\frac{X_{\max}\text{-}X_{\min}}{\text{GSD}}\right)+1 \tag{1}$$

$$\text{Rows} = \text{int}\left(\frac{Y_{\max}\text{-}Y_{\min}}{\text{GSD}}\right)+1 \tag{2}$$

$$\text{Lays} = \text{int}\left(\frac{Z_{\max}\text{-}Z_{\min}}{\text{GSD}}\right)+1 \tag{3}$$

in which, $X_{\max}$, $X_{\min}$, $Y_{\max}$, $Y_{\min}$, $Z_{\max}$, $Z_{\min}$ represent the maximum and minimum values of X, Y and Z coordinates of the point cloud area respectively; GSD is the grid resolution. Cols, Rows, and Lays are the grid column number, row number, and layer number of the cloud points, respectively. The rasterized 3D point cloud is a two-dimensional grid, and each grid contains the elevation value of the location of which the range is between 0–1. In addition, in order to facilitate the subsequent calculation, the elevation value of each grid was multiplied by 255 and rounded to obtain the equivalent grayscale image. In other words, the equivalent grayscale image is the result of refining and simplifying the 3D point cloud and processing it in two dimensions.

3. Pavement texture and fractal dimension calculation

3.1. Profile characteristics of pavement surface

The one-dimensional profile of pavement surface can visually demonstrate the rough condition which is contained in the equivalent grayscale image. In this paper, a row or column in the equivalent grayscale image was randomly selected as a one-dimensional discrete signal, which is regarded as the cross-section contour of the pavement surface. Due to the inevitable noise in the process of 3D reconstruction, the displayed one-dimensional discrete signal will change sharply. Therefore, it needs to be decomposed and reconstructed. In this paper, the original data was decomposed and reconstructed by wavelet analysis based on the Mallat algorithm [30–32]. The calculation procedure is as follows.

First, the wavelet decomposition was carried out to get the signal of each scale according to the original signal f(t). Then, a threshold was selected for soft threshold quantization processing (STQP) of high-frequency signals under various scales. Finally, one-dimensional wavelet reconstruction was carried out by incorporating the low-frequency signal after wavelet decomposition and the high-frequency signal after STQP.

As a matter of fact, the selection of wavelet basis, the number of decomposition layers, and the selection rules of threshold are the key factors that affect the final reconstruction effectiveness. For the selection of wavelet basis, the Daubechies 3 wavelet (db3) was used as the mother wavelet to analyse the pavement image because it contains more local peaks to better represent the typical pavement roughness texture profile [33,34]. For the number of decomposition layers, on the one hand, it should not be too large because it will lead to serious distortion of the reconstructed profile signal; on the other hand, it should not be too small because it will be difficult to distinguish between the noise and the characteristics exhibited by the profile signal. In this paper, the length of the original profile signal is 256 pixels, and the number of decomposition layers was chosen to be three. For one-dimensional profile signals, the standard deviation in the high-frequency signal is usually selected as the threshold for STQP, i.e., the absolute value of the high-frequency signal below the threshold is set to zero, and the absolute value above the threshold is subtracted from the threshold. The decomposed image is

shown in Figure 6. The soft-threshold quantized data of the high-frequency signal is stored in the matrix for reconstruction, and the reconstructed pavement profile is shown in Figure 7.

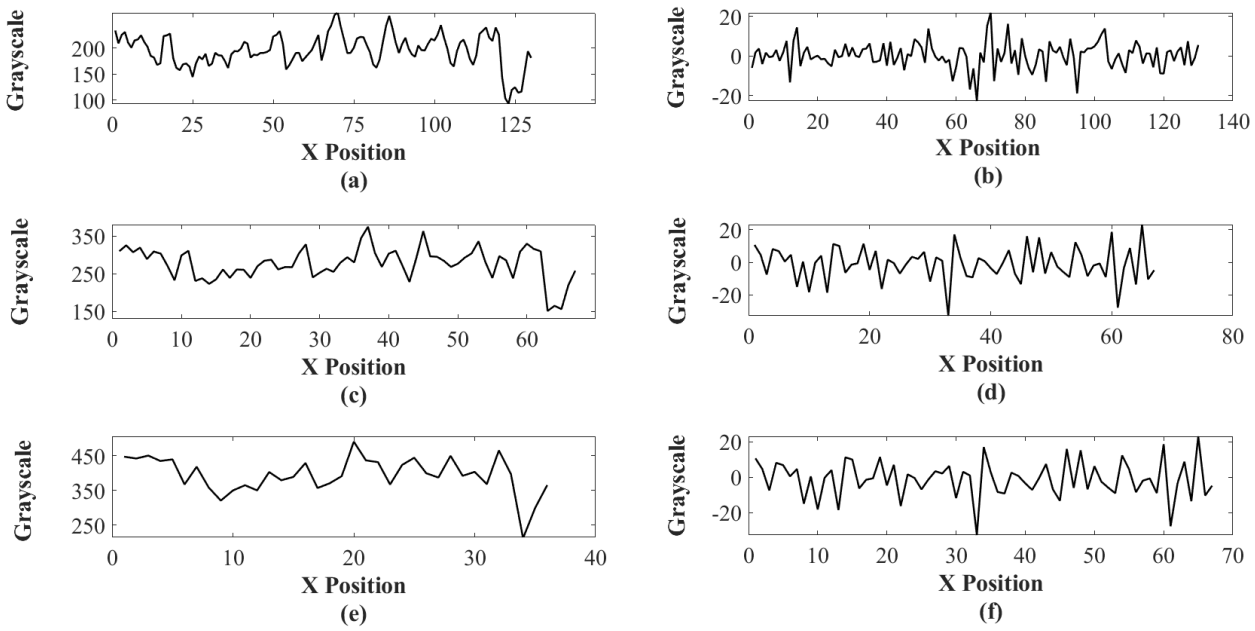

Figure 6. One-dimensional discrete signal decomposition: (a) low-frequency signal of the first decomposition, (b) high-frequency signal of the first decomposition, (c) low-frequency signal of the second decomposition, (d) high-frequency signal of the second decomposition, (e) low-frequency signal of the third decomposition, (f) high-frequency signal of the third decomposition.

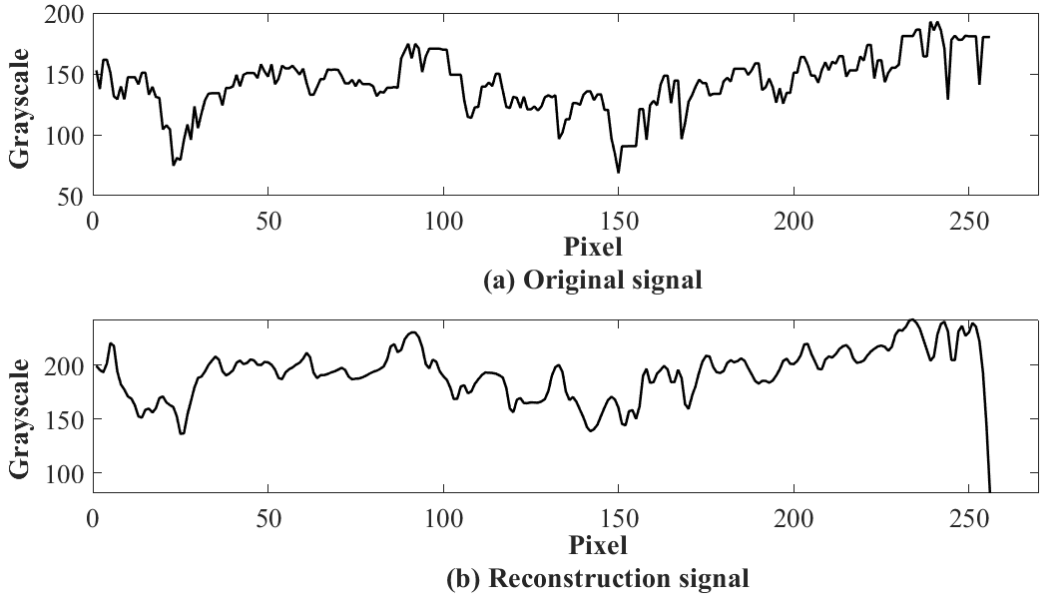

Figure 7. Reconstruction of pavement cross-section profile.

3.2. Fractal dimension of one-dimensional profile

Fractals are used to characterize the self-similarity of objects or quantities at various scales and are usually described by the Fractal Dimension (FD). The cross-sectional profile of asphalt pavement surface has obvious random distribution and complex variability, and its surface texture has been proven to have fractal characteristics in a certain scale range. Therefore, the fractal dimension of the reconstructed pavement surface profile was calculated by the box dimension method (BDM) to quantify the morphological characteristics of asphalt pavement surface and compare it with MTD through the experimental test. The main principle of this method (i.e., BDM) is to place the reconstructed pavement surface profile on an evenly divided grid and calculate the minimum number of grids needed to cover the profile. Then, the fractal dimension FD_1D can be calculated by progressive refinement of the grid to check the change in the number of boxes required to cover it. The results are listed in Table 1.

3.3. Fractal dimension of the two-dimensional pixel matrix

3.3.1. Image pre-processing

There are many studies on asphalt pavement texture based on 2D digital images [35,36], however, there are two problems with the two-dimensional digital image of the asphalt pavement surface. Firstly, the images (photographs) are easily affected by lighting and shooting angle, and the grayscale distribution matrix does not reflect the texture characteristics of the pavement very accurately. Secondly, there is inevitable data loss in the process of converting color images to grayscale images. In addition, due to the equipment, environment, and other reasons, the images are mixed with noise at different degrees during the image acquisition process. Therefore, the images need to be pre-processed with noise reduction before processing by computer. In this paper, two types of processing were performed on the captured pavement images separately. At first, the pavement images were pre-processed with noise reduction, and then the RGB images were grayed out to obtain two-dimensional grayscale images. Secondly, the 3D point cloud was reconstructed based on multi-vision, and the equivalent grayscale image was obtained by coordinate transformation. Then, the noise reduction was conducted by the same method.

For two-dimensional grayscale images and equivalent grayscale images, the method of two-dimensional wavelet decomposition for noise reduction is demonstrated as bellow [37].

Firstly, the mother wavelet and the level N of the wavelet decomposition were selected, and then the decomposition of the signal s should be calculated from the first layer to the Nth decomposition. Next, for each layer from 1 to N, a threshold was selected and a soft threshold quantization of the high-frequency coefficients at this layer was performed. Finally, based on the low-frequency coefficients of the Nth layer of the wavelet decomposition and the modified high-frequency coefficients of each layer from the first layer to the Nth layer, the wavelet reconstruction of the 2-D signal was calculated. As an example, the noise reduction results are shown in Figure 8.

After noise reduction, both two-dimensional grayscale and equivalent grayscale images can be mathematically represented as an $m \times n$ two-dimensional matrix with horizontal coordinates x and vertical coordinates y. If $Z_{i,j} = (x_i, y_j)$, a three-dimensional distribution of grayscale can be illustrated, which represents the surface texture characteristics of asphalt pavement, as shown in Figures 9 and 10.

They are both essentially pixel matrices of size 256 × 256.

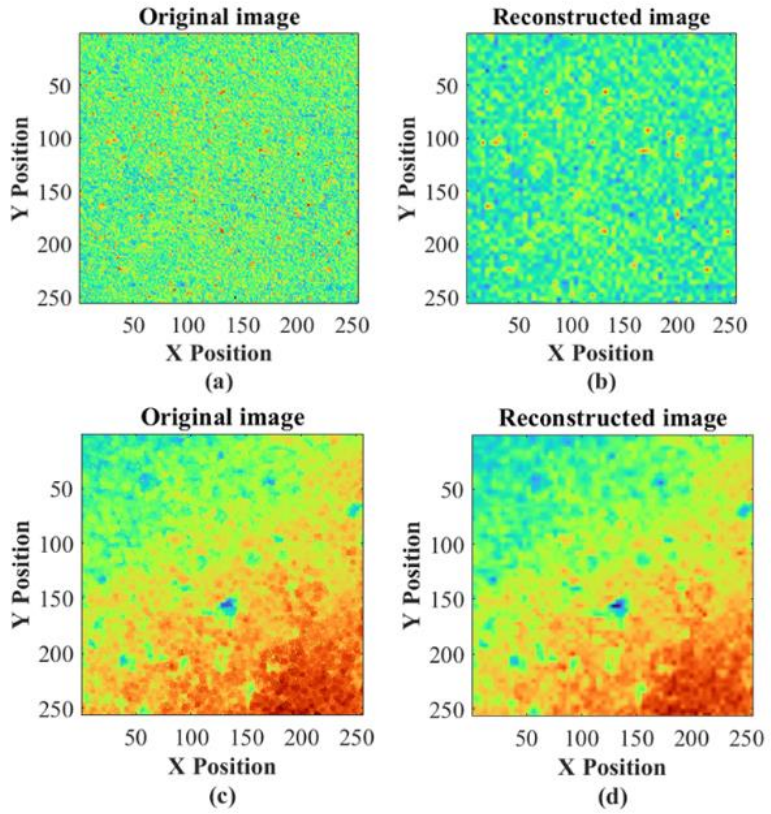

Figure 8. Noise reduction results: (a) original image of 2D grayscale; (b) reconstructed image of 2D grayscale; (c) original image of equivalent grayscale; (d) reconstructed image of equivalent grayscale.

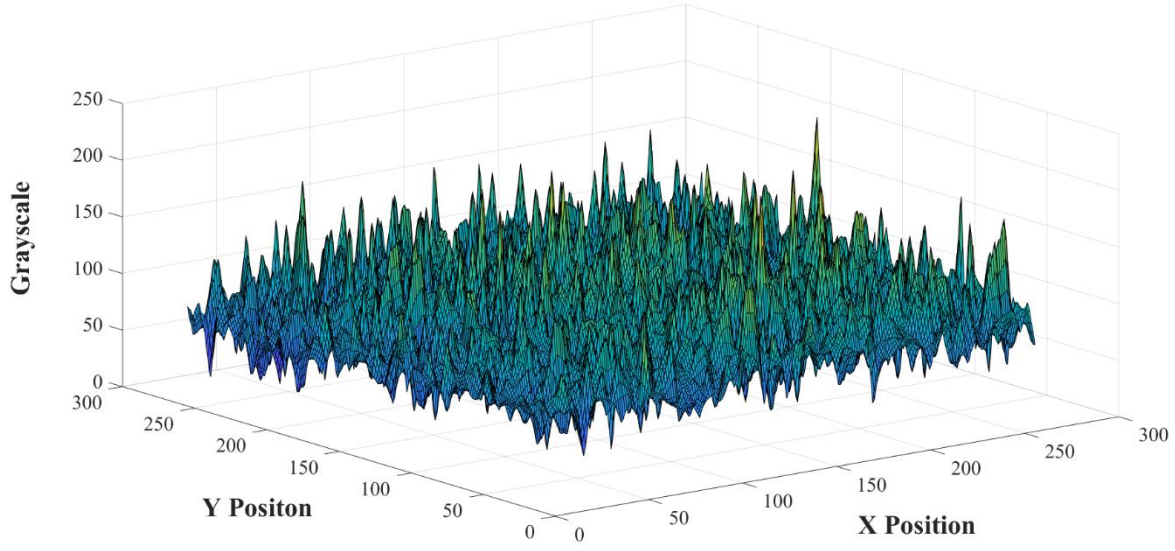

Figure 9. Grayscale distribution of the two-dimensional grayscale image.

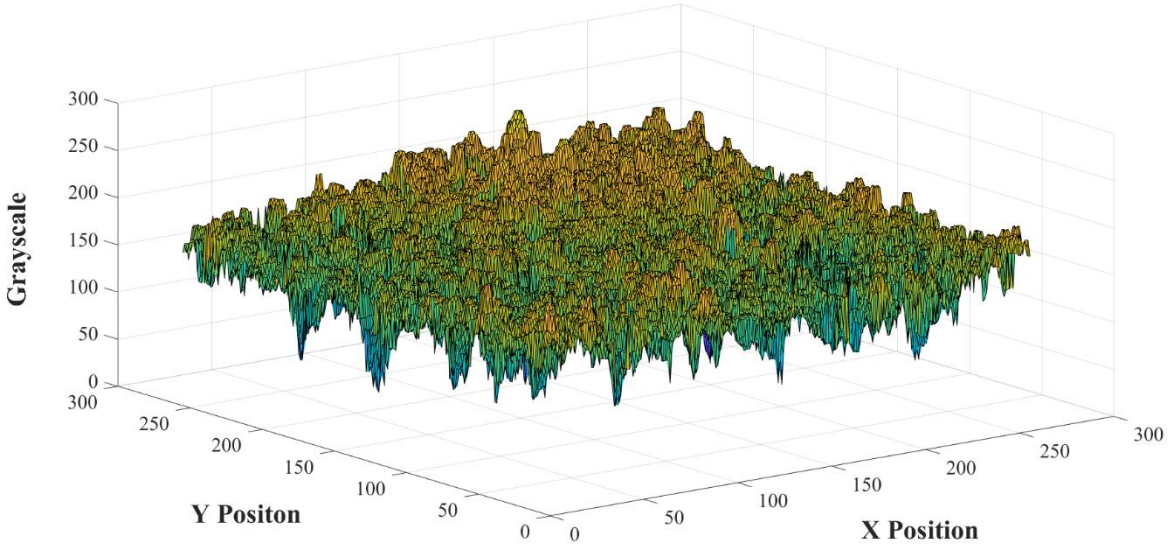

Figure 10. Grayscale distribution of the equivalent grayscale image.

3.3.2. Fractal dimension calculation

The fractal dimension can be used to measure the roughness of the image, also known as the complexity of the grayscale distribution surface. The higher the fractal dimension indicates a more complex surface, and the image will be rougher [38]. For an image of $M \times M$ size, (x,y) represents the position in space in 3D space, and z represents the gray value of its corresponding point gray(x,y). In this paper, the fractal dimension of a two-dimensional grayscale image and equivalent grayscale image were calculated separately using the differential box dimension calculation method as follows:

In the first step, the image was chunked into a grid of $s \times s$ ($M/2 \geq s \geq 2$), where M is the edge length of the vertical projection of the 3D spatial surface, s is the edge length of the cut grid, and s is an integer.

In the second step, in each $s \times s$ chunk, there is a box column, whose size is $s \times s \times s'$ (Figure 11). If the maximum gray value is G, which is usually 256, the box scale is defined as $r = G/s' = M/s$.

In the third step, the maximum gray value and the minimum gray value were calculated for each chunk, which requires k boxes and l boxes to be filled respectively, then $n_r = k - l + 1$.

In the fourth step, the total number of boxes needed to cover the entire surface (Nr) was calculated by

$$N_r = \text{sum}(n_r) \tag{4}$$

The relationship between the total number of counted boxes and the box scale is known from the box dimension principle, as follows:

$$N_r = r^{-FD} \tag{5}$$

Therefore, the fractal dimension can be given by

$$FD = \log(N_r) / \log(\frac{1}{r}) \tag{6}$$

In the fifth step, different grid division sizes were set and a linear fit to the data points was performed using the least squares method to find the linear equation as follows:

$$\log(N_r) = a\ln\left(\frac{1}{r}\right) + b \tag{7}$$

Combined with Eq (6), the slope a in Eq (7) is precisely the fractal dimension (FD). The fractal dimension of the equivalent grayscale image (FD_Ptcloud) and the fractal dimension of the two-dimensional grayscale image (FD_Photo) were calculated respectively.

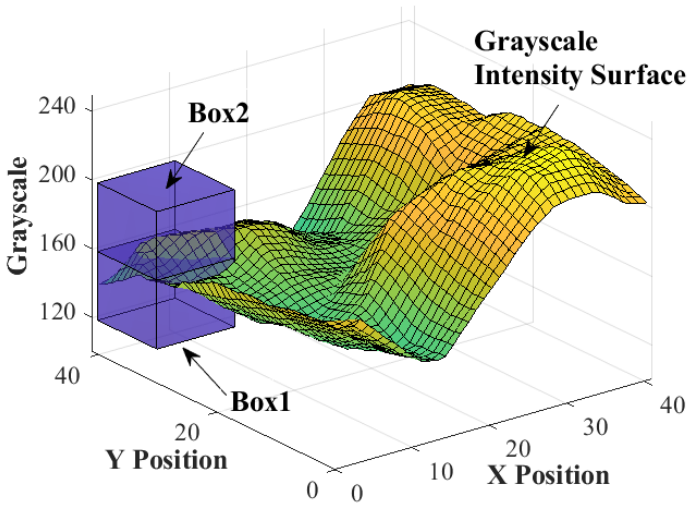

Figure 11. Principle of differential box dimension method.

4. Results and discussions

4.1. MTD by sand spreading method

The sand spreading method is used to obtain the mean texture depth (MTD) to validate the method of fractal dimension and characterize the pavement texture characteristics. In this paper, 30 measurement points were selected to detect and calculate the MTD of pavement surface of the Zhutang West Road (Located in Hunan Province, China). As shown in Figure 12, the clean fine sand with particle size ranging from 0.15 to 0.3 *mm* and total volume V was spread evenly on the test points, and the pusher plate with rubber sheet glued on the bottom was used to repeat the paving motion from inside to outside until the sand fills in the gap of the rough pavement surface, and the sand was spread to form a circle as outwards as possible. Then, the horizontal and vertical diameters D_1 and D_2 of the formed circle were measured with a steel ruler, and the average value was taken as D. Finally, the mean texture depth of all measurement points can be calculated by the Eq (5).

$$\mathrm{MTD} = \frac{4\mathrm{V}}{\pi \mathrm{D}^2} \tag{8}$$

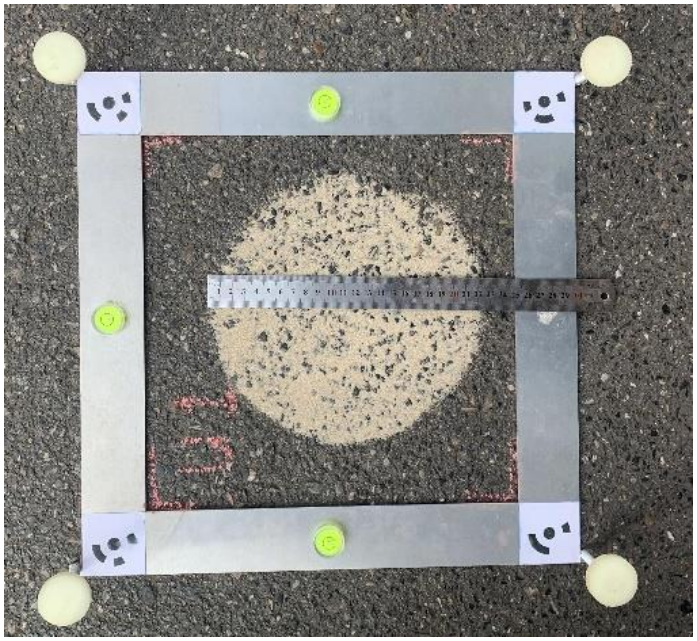

Figure 12. Schematic diagram of sand spreading method.

4.2. Correlation between MTD and fractal dimension

Based on the image data and point cloud data of 30 pavement measurement points, the 1D pavement profile, 2D grayscale image, and equivalent grayscale image were obtained respectively. According to the method described in Section 3, the fractal dimensions of pavement texture were calculated separately by programming. The results of the fractal dimension and MTD of 30 pavement measurement points are listed in Table 1. The relation between fractal dimension and MTD is illustrated in Figures 13–15, respectively.

It can be seen from Figure 13 that there is a positive correlation between the fractal dimension of the one-dimensional pavement surface profile and the mean texture depth, i.e., the larger the fractal dimension represents the rougher pavement surface, and the MTD is greater accordingly. It can be assumed that the fractal dimension can characterize the texture information of the pavement to some extent. However, this kind of correlation is not very obvious (e.g., $R^2 = 0.61454$).

From the comparison between Figures 14 and 15, the fractal dimension of an equivalent grayscale image and MTD has better relationship ($R^2 = 0.8383$). As a matter of fact, a two-dimensional grayscale image is more likely to be influenced by the pavement surface color, because the essence of a two-dimensional grayscale image is converted from an RGB image. In the two-dimensional grayscale image, different colors of pavement surface will lead to large fluctuations in the value of grayscale, and then the calculated height difference between two adjacent points is inconsistent with the actual situation. On the contrary, the equivalent grayscale image is transformed from the reconstructed 3D point cloud, and the grayscale value of each point represents the elevation of different pavement surfaces. Therefore, the equivalent grayscale image can better reflect the real roughness of the pavement surface.

Table 1. Pavement texture depth and fractal dimension of the West Zhutang Road.

Measurement point number	*MTD* (*mm*)	FD-1D*	FD-Photo**	FD-Ptcloud***
U1	0.6517	1.3565	2.5245	2.4616
U2	0.5619	1.3431	2.5127	2.3902
U3	0.5813	1.3630	2.5386	2.4226
U4	0.5715	1.3390	2.5603	2.4387
U5	0.6069	1.3305	2.5617	2.4609
U6	0.6315	1.2989	2.5387	2.4816
U7	0.5302	1.3570	2.5761	2.3838
U8	0.6953	1.3737	2.5486	2.4507
U9	0.5715	1.3569	2.5513	2.4277
U10	0.5965	1.3389	2.5193	2.4544
V1	0.5715	1.3376	2.5071	2.4145
V2	0.5595	1.3607	2.5660	2.4492
V3	0.6069	1.3459	2.5211	2.4308
V4	0.6017	1.3542	2.5851	2.4414
V5	0.5965	1.3503	2.6194	2.4067
V6	0.5072	1.3099	2.5257	2.4009
V7	0.5813	1.3444	2.5860	2.4772
V8	0.6538	1.3764	2.5924	2.4791
V9	0.5526	1.3210	2.6330	2.4036
V10	0.5572	1.3236	2.5941	2.3924
W1	0.6096	1.3432	2.5793	2.494
W2	0.5739	1.3575	2.5287	2.4841
W3	0.5739	1.3627	2.5540	2.4654
W4	0.6372	1.3316	2.5434	2.4896
W5	0.5346	1.3328	2.5356	2.4254
W6	0.6487	1.3483	2.5659	2.5221
W7	0.8899	1.4395	2.6585	2.6335
W8	0.7611	1.3636	2.6297	2.575
W9	0.8414	1.4008	2.6312	2.6216
W10	0.8371	1.4096	2.6313	2.5953

FD-1D* represents the fractal dimension of one-dimensional pavement section profile;
FD-Photo** represents the fractal dimension of two-dimensional grayscale image
FD-Ptcloud*** represents the fractal dimension of equivalent grayscale image

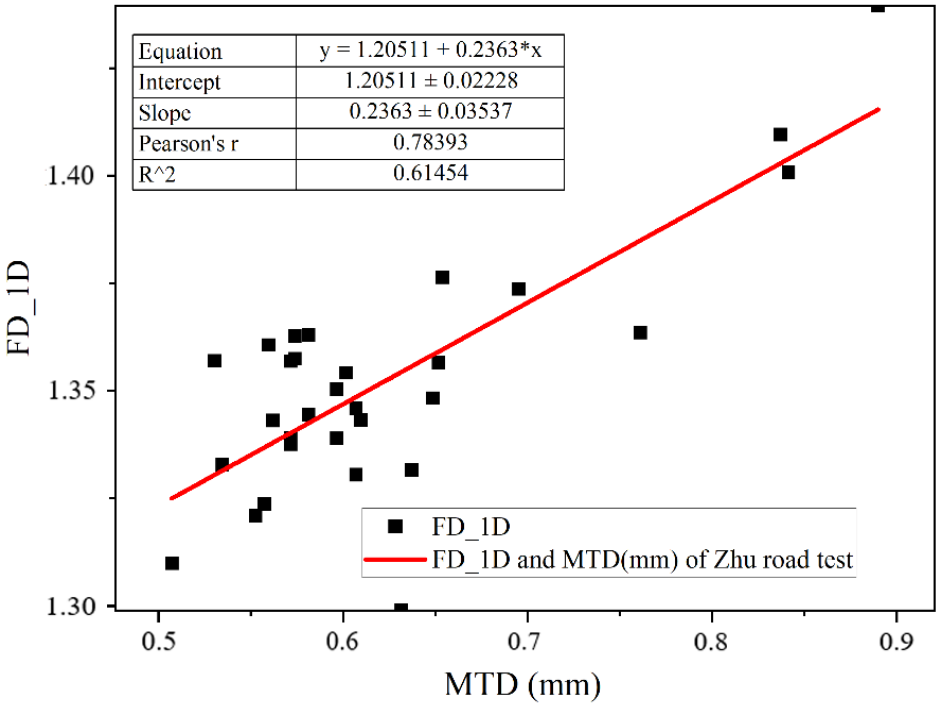

Figure 13. Correlation between MTD and fractal dimension of one-dimensional pavement section profile.

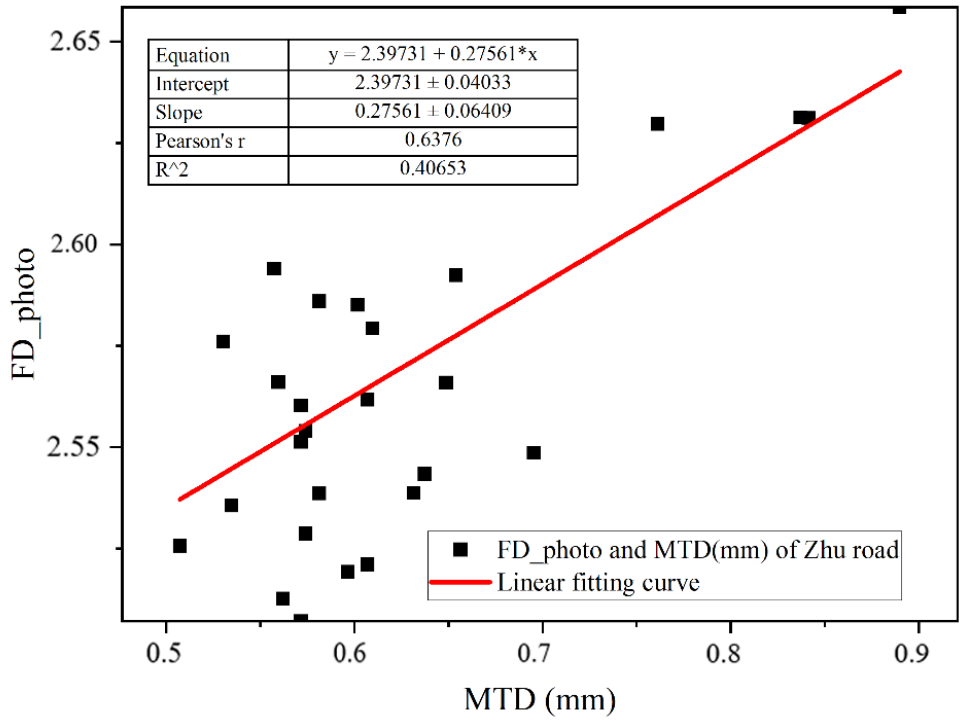

Figure 14. Correlation between MTD and fractal dimension of two-dimensional grayscale image.

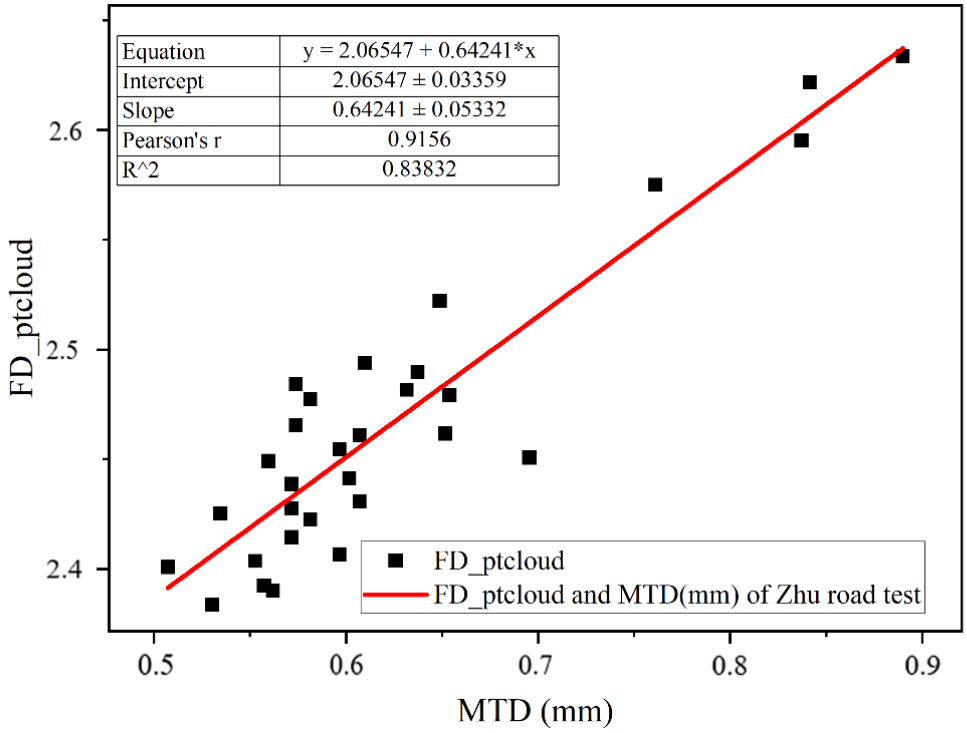

Figure 15. Correlation between MTD and fractal dimension of equivalent grayscale image.

It should be pointed out that about 20~30 photos were taken at each test point in this paper, and the shooting time of each photo was about 3 seconds. Therefore, each test point takes between 1 and 2 minutes. As for the sand patch method, it takes at least 10 minutes for one measuring point from preparation to completion. As a matter of fact, a modest reduction in the number of photos taken (e.g., 10 high-definition images) can also achieve the same accuracy, depending on the quality of the images taken. If the photo quality is high enough, the number of photos required is lower, and the shooting time can be further reduced. Therefore, the method proposed in this paper has obvious advantages in terms of efficiency. Compared with the existing image processing methods, the proposed method in this paper makes full use of the depth information of the shot image to determine the texture depth of pavement more accurately. However, at current stage, the method can only be used at a fixed point like the sand patch method, which affects the normal traffic passage (i.e., the lane closure is required). If an integrated device is developed in the future and high-performance cameras from different angles are integrated in the front of the vehicle (e.g., the cameras have functions of high-definition, high-sensitive photography, and quick photography), all cameras can shoot simultaneously, which will greatly reduce the shooting time. Therefore, the method proposed in this paper will continue to carry out research in the field of image synthesis and reconstruction to obtain the pavement texture image continuously, accurately and efficiently.

5. Conclusions

This paper aims to investigate the fractal characteristics of asphalt pavement texture roughness incorporating 3D reconstruction technology. In this paper, three-dimensional image reconstruction,

three-dimensional point cloud rasterization, and wavelet decomposition theory, were applied for pavement image processing. The new technical process was proposed from two-dimensional pavement image to three-dimensional reconstruction point cloud, and then to equivalent grayscale images. Furthermore, the calculation of fractal dimension under different conditions and analysis of pavement roughness were carried out. The main conclusions can be drawn as bellow.

1) Based on the technology of multiocular vision integrating photographs from different shooting angles, the 3D reconstruction of pavement surface morphology was carried out by the SFM method to establish a pavement texture model. Through rasterization, the disordered and huge number of 3D point clouds were transformed into equivalent grayscale images which contain the pavement texture information in the form of a data matrix.

2) Based on the equivalent grayscale image, the db3 wavelet was used as the mother wavelet to decompose the one-dimensional pavement section profile, and then the pavement profile is reconstructed after soft threshold quantization processing to calculate its fractal dimension. It is found that the fractal dimension has a positive correlation with the MTD, and the larger the fractal dimension, the greater the roughness of pavement surface.

3) The fractal dimensions of equivalent grayscale and two-dimensional grayscale were calculated based on the difference box dimension method. By comparing the correlation degree between the two fractal dimensions and the actual pavement MTD, it can be found that the fractal dimension of two-dimensional grayscale is generally higher than that of equivalent grayscale, and the fractal dimension of equivalent grayscale has a better correlation with MTD.

4) The equivalent grayscale image was directly transformed by the reconstruction of the three-dimensional point cloud, and the grayscale value of each point represents the elevation of different pavement surfaces. Therefore, the equivalent grayscale image can better reflect the real roughness of the pavement surface.

In this paper, an efficient evaluation method for asphalt pavement texture was proposed and validated by on-site test. The calculation results showed that the fractal dimension of pavement fits well with MTD, which provides a potential reference for quantifying asphalt pavement texture. Compared with traditional methods, the method in this paper overcome the problem of insufficient accuracy in extracting pavement texture information from 2D digital images and solved the problem of redundant and difficult to calculate 3D point cloud data. However, to provide enough data to construct the 3D point cloud (Figure 5), some photos must be taken. Therefore, these pavement condition evaluations should be made from one point to another, and it would not be possible to obtain data in continuous way, as other devices are able to do, which needs further to be studied to improve the accuracy of the proposed method in the future.

Acknowledgments

This work was funded by the National Natural Science Foundation of China (Grant No.52278468; U22A20235), the Natural Science Foundation of Hunan Province (CN) (Grant No. 2020JJ4702). The authors appreciate the financial support from Hunan Expressway Group Co. Ltd and the Hunan Department of Transportation (No. 202152) in China, as well as the funding support from the Beijing high-level overseas talents returned to China.

Conflict of interest

The authors declare there is no conflict of interest.

References

1. Y. Jia, S. Wang, J. Peng, Y. Gao, D. Hu, X. Zhao, Evaluation of pavement rutting based on driving safety of vehicles, *Int. J. Pavement Res. Technol.*, **15** (2022), 457–469. https://doi.org/10.1007/s42947-021-00032-2
2. P. Buddhavarapu, A. Banerjee, J. A. Prozzi, Influence of pavement condition on horizontal curve safety, *Accid. Anal. Prevent.*, **52** (2013), 9–18. https://doi.org/10.1016/j.aap.2012.12.010
3. J. Hu, X. Gao, R. Wang, S. Sun, Research on comfort and safety threshold of pavement roughness, *Transp. Res. Record*, **2641** (2017), 149–155. https://doi.org/10.3141/2641-17
4. T. Wang, L. Hu, X. Pan, S. Xu, D. Yun, Effect of the compactness on the texture and friction of asphalt concrete intended for wearing course of the road pavement, *Coatings*, **10.2** (2020), 192. https://doi.org/10.3390/coatings10020192
5. H. Pérez-Acebo, H. Gonzalo-Orden, D. J. Findley, E. Rojí, A skid resistance prediction model for an entire road network, *Constr. Build. Mater.*, **262** (2020), 120041. https://doi.org/10.1016/j.conbuildmat.2020.120041
6. Y. Peng, J. Q. Li, Y. Zhan, K. C. P. Wang, G. Yang, Finite element method-based skid resistance simulation using in-situ 3D pavement surface texture and friction data, *Materials*, **12** (2019), 3821. https://doi.org/10.3390/ma12233821
7. D. Chen, N. R. Sefidmazgi, H. Bahia, Exploring the feasibility of evaluating asphalt pavement surface macro-texture using image-based texture analysis method, *Road Mater. Pavement Design*, **16** (2015), 405–420. https://doi.org/10.1080/14680629.2015.1016547
8. F. G. Praticò, R. Vaiana, A study on the relationship between mean texture depth and mean profile depth of asphalt pavements, *Constr. Build. Mater.*, **101** (2015), 72–79. https://doi.org/10.1016/j.conbuildmat.2015.10.021
9. J. Huyan, W. Li, S. Tighe, Z. Sun, Quantitative analysis of macrotexture of asphalt concrete pavement surface based on 3D data, *Transp. Res. Record*, **2674** (2020), 732–744. https://doi.org/10.1177/0361198120920269
10. D. W. Bechert, M. Bruse, W. Hage, R. Meyer, Fluid mechanics of biological surfaces and their technological application, *Naturwissenschaften*, **87** (2000), 157–171. https://doi.org/10.1007/s001140050696
11. S. Chen, X. Liu, H. Luo, J. Yu, F. Chen, Y. Zhang, A state-of-the-art review of asphalt pavement surface texture and its measurement techniques, *J. Road Eng.*, **2** (2022), 156–180. https://doi.org/10.1016/j.jreng.2022.05.003
12. L. F. Walubita, E. Mahmoud, S. I. Lee, G. Carrasco, J. J. Komba, J. J. Komba, Use of grid reinforcement in HMA overlays–A Texas field case study of highway US 59 in Atlanta District, *Constr. Build. Mater.*, **213** (2019), 325–336. https://doi.org/10.1016/j.conbuildmat.2019.04.072
13. O. H. Jeong, D. H. Chen, L. F. Walubita, A. J. Wimsatt, Mitigating seal coat damage due to superheavy load moves in Texas low volume roads, *Constr. Build. Mater.*, **25** (2011), 3236–3244. https://doi.org/10.1016/j.conbuildmat.2011.03.010

14. L. Fuentes, K. Taborda, X. Hu, E. Horak, T. Bai, L. F. Walubita, A probabilistic approach to detect structural problems in flexible pavement sections at network level assessment, *Int. J. Pavement Eng.*, **78** (2020), 1867–1880. https://doi.org/10.1080/10298436.2020.1828586
15. A. E. Gendy, A. Shalaby, Mean profile depth of pavement surface macrotexture using photometric stereo techniques, *J. Transp. Eng.*, **133** (2007), 433–440. https://doi.org/ 10.1061/(ASCE)0733-947X(2007)133:7(433)
16. Z. Du, J. Yuan, F. Xiao, C. Hettiarachchi, Application of image technology on pavement distress detection: A review, *Measurement*, **184** (2021), 109900. https://doi.org/10.1016/j.measurement.2021.109900
17. L. Liu, P. Zhu, J. Guan, R. Jiang, X. Zhou, A binocular reconstruction method fused with Laplacian image information for pavement texture evaluation, *Measurement*, **185** (2021), 110039. https://doi.org/10.1016/j.measurement.2021.110039
18. I. Pranjić, A. Deluka-Tibljaš, Pavement texture-friction relationship establishment via image analysis methods, *Materials*, **15** (2022), 846. https://doi.org/10.3390/ma15030846
19. L. Puzzo, G. Loprencipe, C. Tozzo, A. D'Andrea, Three-dimensional survey method of pavement texture using photographic equipment, *Measurement*, **111** (2017), 146–157. https://doi.org/10.1016/j.measurement.2017.07.040
20. K. Zhang, P. Sun, L. Li, Y. Zhao, Y. Zhao, Z. Zhang, A novel evaluation method of aggregate distribution homogeneity for asphalt pavement based on the characteristics of texture structure, *Constr. Build. Mater.*, **306** (2021), 124927. https://doi.org/10.1016/j.conbuildmat.2021.124927
21. O. Ghaderi, M. Abedini, Evaluation of the airport runway flexible pavement macro-texture using digital image processing technique (DIPT), *Int. J. Pavement Eng.*, **23** (2021), 1–13. https://doi.org/10.1080/10298436.2021.1968393
22. H. C. Dan, G. W. Bai, Z. H. Zhu, X. Liu, W. Cao, An improved computation method for asphalt pavement texture depth based on multiocular vision 3D reconstruction technology, *Constr. Build. Mater.*, **321** (2022), 126427. https://doi.org/10.1016/j.conbuildmat.2022.126427
23. S. Green, A. Bevan, M. Shapland, A comparative assessment of structure from motion methods for archaeological research, *J. Archaeol. Sci.*, **46** (2014), 173–181. https://doi.org/10.1016/j.jas.2014.02.030
24. Y. Ding, X. Zheng, Y. Zhou, H. Xiong, J. Gong, Low-cost and efficient indoor 3D reconstruction through annotated hierarchical structure-from-motion, *Remote Sens.*, **11** (2018), 58–68. https://doi.org/10.3390/rs11010058
25. S. Zhao, D. D. Robeltson, G. Wang, B. Whiting; K. T. Bae, X-ray CT metal artifact reduction using wavelets: an application for imaging total hip prostheses, *IEEE Trans. Med. Imaging*, **19** (2000), 1238–1247. http://dx.doi.org/10.1109/42.897816
26. S. W. Hasinoff, D. Sharlet, R. Geiss, A. Adams, J. T. Barron, F. Kainz, Burst photography for high dynamic range and low-light imaging on mobile cameras, *ACM Trans. Graphics (ToG)*, **35** (2016), 1–12. https://doi.org/10.1145/2980179.2980254
27. A. O. Akyüz, Deep joint deinterlacing and denoising for single shot dual-ISO HDR reconstruction, *IEEE Trans. Image Process.*, **29** (2020), 7511–7524. https://doi.org/10.1109/TIP.2020.3004014
28. Z. J. Burk, C. S. Johnson, Method for production of 3D interactive models using photogrammetry for use in human anatomy education, *HAPS Educ.*, **23** (2019), 457–463. https://doi.org/10.21692/HAPS.2019.016

29. G. Jakovljevic, M. Govedarica, F. Alvarez-Taboada, V. Pajic, Accuracy assessment of deep learning-based classification of LiDAR and UAV points clouds for DTM creation and flood risk mapping, *Geosciences*, **9** (2019), 323. https://doi.org/10.3390/geosciences9070323
30. H. Wendt, P. Abry, S. Jaffard, H. Ji, Z. Shen, Wavelet leader multifractal analysis for texture classification, in *2009 16th IEEE International Conference on Image Processing (ICIP)*, (2009), 3829–3832. https://doi.org/10.1109/ICIP.2009.5414273.
31. S. Mallat, Zero-crossings of a wavelet transform, *IEEE Trans. Inf. Theory*, **37** (1991), 1019–1033. https://doi.org/10.1109/18.86995
32. G. Strang, Wavelet transforms versus Fourier transforms, *Bull. Am. Math. Soc.*, **28** (1993), 288–305. https://doi.org/10.1090/s0273-0979-1993-00390-2
33. G. Yang, Q. J. Li, Y. J. Zhan, K. C. P. Wang, C. Wang, Wavelet based macrotexture analysis for pavement friction prediction, *KSCE J. Civ. Eng.*, **22** (2018), 117–124. https://doi.org/10.1007/s12205-017-1165-x
34. L. Wei, T. F. Fwa, Z. Zhe, Wavelet analysis and interpretation of road roughness, *J. Transp. Eng.*, **131** (2005), 120–130. https://doi.org/10.1061/(ASCE)0733-947X(2005)131:2(120)
35. T. Wan, H. Wang, P. Feng, A. Diab, Concave distribution characterization of asphalt pavement surface segregation using smartphone and image processing based techniques, *Constr. Build. Mater.*, **301** (2021), 124111. https://doi.org/10.1016/j.conbuildmat.2021.124111
36. M. M. Kanafi, A. Kuosmanen, T. K. Pellinen, A. J. Tuononen, Macro-and micro-texture evolution of road pavements and correlation with friction, *Int. J. Pavement Eng.*, **16** (2015), 168–179. https://doi.org/10.1080/10298436.2014.937715
37. M. Abdulkareem, N. Bakhary, M. Vafaei, N. M. Noor, R. N. Mohamed, Application of two-dimensional wavelet transform to detect damage in steel plate structures, *Measurement*, **146** (2019), 912–923. https://doi.org/10.1016/j.measurement.2019.07.027
38. C. Liu, Y. Zhan, Q. Deng, Y. Qiu, A. Zhang, An improved differential box counting method to measure fractal dimensions for pavement surface skid resistance evaluation, *Measurement*, **178** (2021), 109376. https://doi.org/10.1016/j.measurement.2021.109376

AIMS Press